Chemical Science

ROYAL SOCIETY OF CHEMISTRY

EDGE ARTICLE

View Article Online
View Journal



Cite this: DOI: 10.1039/d6sc00024j

All publication charges for this article have been paid for by the Royal Society of Chemistry



# Influence of molecular shape and hydrogen bonding on glycolipid self-assembly into thermotropic gyroid phases

Soumi Das, [a] Caini Zheng,[a] Timothy P. Lodge, [ab] J. Ilja Siepmann, [a] Michelle A. Calabrese [*b] and Theresa M. Reineke [*ab]

Periodic network morphologies such as the double gyroid (DG) are promising for a wide range of applications, from optical materials and organic semiconductors to separation membranes and drug delivery vehicles. While natural glycolipids are a constituent of cell membranes, synthetic glycolipids have emerged as candidates for producing thermotropic DG phases with sub-5 nm domains. Despite this potential, difficulties in producing stereochemically-pure glycolipids and a lack of known design rules governing DG self-assembly limit their broad use. Our recent work identified two key factors stabilizing DG in ten anomerically pure Guerbet cellobiosides: a bent molecular topology and moderate hydrogen bonding between sugar headgroups. However, the influence of glycolipid shape *vs.* hydrogen bonding could not be decoupled, as these factors depend on both headgroup and anomeric stereochemistry. To disentangle these effects, we synthesized 20 anomerically-pure Guerbet glycolipids with different disaccharide headgroups (lactose, maltose) and Guerbet tails ($C_8$–$C_{24}$) and compared them with ten similar cellobiosides. Analysis of the thermotropic phase behavior using differential scanning calorimetry, polarized optical microscopy, small-angle X-ray scattering, and complementary molecular simulations identified numerous cases of DG phase formations, with phase stability dependent on headgroup type and anomeric stereochemistry. With respect to molecular shape, high stability DG phases were promoted by molecules with kinks in topology at similar positions; the most stable DG phases also shared similar inter-molecular hydrogen bonding motifs between specific headgroup hydroxyls. Beyond revealing design guidelines for producing DG phases, this comprehensive understanding of glycolipid self-assembly may accelerate development of biomimetic materials, as the liquid crystalline behavior of natural glycolipids plays a pivotal role in biological functions.

Received 3rd January 2026
Accepted 17th March 2026

DOI: 10.1039/d6sc00024j

rsc.li/chemical-science

## Introduction

Network morphologies resulting from the spontaneous organization of biomolecular building blocks are ubiquitous in nature.[1,2] The intriguing network structure, with its remarkable properties such as the formation of photonic crystals[1–4] and impact-resistant materials,[5] has inspired the design of novel materials for optical materials,[6] organic semiconductors,[7] separation membranes,[8] energy storage,[9] tissue engineering,[10] therapeutic delivery,[11] and many other areas.[12] Among these morphologies, three-dimensional periodic network morphologies (NET) like the cubic DG and double diamond are particularly interesting due to their bicontinuous and interpenetrating network structures, which are highly advantageous for diverse applications. To achieve bottom-up synthesis of materials with such intricate structures, self-assembly of amphiphiles has emerged as a promising route for the next generation of materials processing.

Various liquid crystal (LC) mesogens, including block copolymers,[13] rod-like polyphiles,[14,15] wedge-shaped molecules,[16] disc-like molecules,[17] bolamphiphiles,[18,19] and glycolipids[20,21] are recognized for their ability to form thermotropic DGs in the absence of solvent. The amphiphile size and design play a crucial role in determining DG length scales. To address challenges associated with miniaturizing developed technologies, there is a growing demand for reducing the DG feature sizes. Furthermore, specific applications of DG materials, such as nanofiltration, nanopatterning, microelectronics, drug delivery, and others, mandate a feature size below 5 nm.[22,23] While a few designs have been developed to achieve sub-10 nm feature sizes from polymeric amphiphiles,[24–28] employing glycolipids or small molecule amphiphiles offers a readily attainable solution. Glycolipids, abundant in nature and found in the cell membranes of all living systems,[29,30] are not only a sustainable source but also contribute to material biodegradability.

[a]Department of Chemistry, University of Minnesota Twin Cities, 207 Pleasant St SE, Minneapolis, MN 55455, USA. E-mail: treineke@umn.edu; mcalab@umn.edu
[b]Department of Chemical Engineering and Materials Science, University of Minnesota Twin Cities, 421 Washington Ave SE #151, Minneapolis, MN 55455, USA

A primary hurdle in developing DG materials is ensuring stability of the self-assembled structure. This challenge stems from the intricate geometric arrangement of DG phases, featuring saddle-shaped interfaces in which the negative Gaussian curvature undergoes periodic changes from the NET connectors to the struts. Numerous amphiphile designs have been proposed for forming or stabilizing thermotropic DGs. In polymeric amphiphiles, these approaches include shape-filling ABC triblock polymers,[31,32] coil–brush/bottlebrush polymers,[33–35] and modulation of various molecular parameters.[36,37] For small molecular amphiphiles, achieving thermotropic DGs involves T- and X-shaped,[38,39] polycatenar,[40] or π-conjugated rod-like molecules.[14]

While prior work has reported thermotropic DGs in glycolipids,[41] a comprehensive assessment of glycolipid phase behavior is lacking, limiting the establishment of robust design principles and constraining potential applications. Conversely, several strategies have been used to stabilize glycolipid-based DGs in lyotropic conditions.[42–44] While exploration of glycolipid structures responsible for thermotropic DG formation has mainly focused on monosaccharide-based lipids, their DG thermal stability window is narrow (~12–35 °C, Table S1). In contrast, disaccharide-based lipids can form thermotropic cubic phases over moderate temperature ranges.[45,46] Vill *et al.* identified cubic phases for a variety of straight-chain disaccharide-based lipids,[45] and Hashim *et al.* reported DG in a maltose-based glycolipid with a $-C_{14}C_{10}$ Guerbet branched tail (Table S1).[46] These irregularly-shaped, branched Guerbet tails have also been used to induce DG with monosaccharide headgroups.[47]

Beyond headgroup and tail identity, glycolipid headgroup and anomeric stereochemistry alter self-assembly, particularly in monosaccharide lipids.[48–51] However, exploration of the stereochemistry-dependent self-assembly in disaccharide-based lipids is scarce. While Hashim *et al.*[52,53] examined the role of headgroup stereochemistry on the thermotropic phase behavior of lipids including maltose, lactose, and cellobiose, the specific cubic packings and associated domain spacings were not identified for most compounds.[53] Similarly, Vill *et al.* highlighted differences in phase behavior for a few pairs of disaccharide lipid anomers, but the specific cubic phases and associated length scales were not characterized.[45] The impact of anomeric stereochemistry on the self-assembly of disaccharide lipids has likely been overlooked due to limited reports on α-anomers. Accordingly, most current literature only delves into the synthesis and phase behaviors of β-anomers.[53]

Recently, Das and co-workers identified a profound impact of anomeric stereochemistry on the thermotropic self-assembly of a cellobiose-based glycolipid series with Guerbet tails.[54] For α- and β-anomers of certain tail lengths, the shape irregularity imparted by the tails was sufficient to destabilize constant mean curvature packings such as lamellae (LAM) and hexagonally-packed cylinders (HEX), in favor of DG. However, while both anomers formed stable network phases for certain Guerbet tail lengths, the β-anomers formed stable DG phases with shorter tails ($-C_{10}C_6$) than the α-anomers ($-C_{12}C_8$, $-C_{14}C_{10}$). Interestingly, DG structures formed by α-$C_{14}C_{10}$ cellobiose had an exceptionally high temperature stability window of 78 °C. Supporting molecular dynamics (MD) simulations on LAM-forming α- and β-anomers revealed two key differences between the anomers: (1) α-anomers assumed a bent, "boomerang" shape that packed less regularly than the comparatively planar β-anomers; and (2) hydrogen bonding between the cellobiose headgroups was weaker for α-anomers, which allowed the α-anomers to access a higher number of conformations upon packing. While this work established a key role for both molecular shape and headgroup hydrogen bonding in destabilizing planar bilayer packings, the relative importance of each factor could not be determined because only one sugar headgroup was investigated. As such, both molecular shape and hydrogen bonding changed with anomeric stereochemistry and could not be altered individually. These findings motivated the design of a new series of Guerbet glycolipids, where the glycolipid shape and headgroup hydrogen bonding can be systematically altered *via* anomeric position and specific sugar head.

In this work, we uncover the precise role of headgroup hydrogen bonding *vs.* molecular shape on thermotropic self-assembly and stabilization of DG phases in disaccharide Guerbet glycolipids. To do so, we judiciously selected, carefully synthesized, and purified a series of glycolipids employing two disaccharide headgroups – maltose and lactose – with Guerbet tails ($-C_6C_2$ to $-C_{14}C_{10}$) attached in an anomerically pure manner. This work is the first to examine the thermotropic phase behaviors of Guerbet α-lactosides and α-maltosides and show that unlike the β-anomers, none of these α-anomers were able to stabilize a DG phase with the higher chain lengths ($-C_{12}C_8$ and $-C_{14}C_{10}$), overcoming a significant limitation in the field.[53] Here, molecular shape is controlled by the stereochemistry of both the tail and glycosidic bond between the two monosaccharide units; hydrogen bonding is controlled *via* the stereochemistry of the C4′ hydroxyl group. The α- and β-lactose-based glycolipids have a similar molecular shape to α- and β-cellobiose-based Guerbet glycolipids in our prior work but a different orientation of the C4′ hydroxyl group; conversely, the C4′ hydroxyl group is unchanged for maltose- *vs.* cellobiose-based glycolipids, but the headgroup shape changes based on headgroup glycosidic bond stereochemistry. Using differential scanning calorimetry (DSC), polarized optical microscopy (POM), and small-angle X-ray scattering (SAXS), we uncover the impact of headgroup structure, anomeric stereochemistry, and hydrogen bonding on self-assembly, focusing on DG formation and thermal stability. Complementary MD simulations reveal how shape irregularity and intermolecular headgroup hydrogen bonding work in tandem to enhance thermal DG stability. These insights provide fundamental principles for forming stable network phases in glycolipids and guide the design of molecules that reliably assemble into network phases.

## Results and discussion

To understand the relative importance of molecular shape *vs.* headgroup hydrogen bonding in stabilizing network phases, a series of anomerically-pure α- and β-Guerbet glycolipids with maltose and lactose headgroups (Fig. 1) were synthesized, with

tails ranging in length from $-C_6C_2$ to $-C_{14}C_{10}$ and their phase behavior is compared with that of cellobioside compounds with identical tail lengths taken from our prior work.[54]

### Glycolipid synthesis

All the lactose- and maltose-containing glycolipids were synthesized by traditional Lewis acid-mediated glycosylation procedures using the peracetylated disaccharides and Guerbet alcohols of the type $HOCH_2CHR_1R_2$ ($R_1$=$C_{2m+2}H_{4m+5}$ and $R_2$=$C_{2m}H_{4m+1}$, $m$ = 1–5). For achieving anomerically pure glycolipids with a modest yield, the Lewis acid was chosen judiciously with subsequent optimization of reaction time (Scheme 1) consistent with our previously published strategy for synthesizing anomerically pure Guerbet cellobiosides.[54] Per prior literature,[45,53] using $BF_3\cdot Et_2O$ and $SnCl_4$ as the Lewis acid along with an optimized reaction time ensured the yield of either β- or α-dominant anomeric mixtures, enabling purification of the specific anomer with adequate yield. In general, for both lactose and maltose-based glycolipids, 4 h glycosylation with $BF_3\cdot Et_2O$ was sufficient to produce β-anomers exclusively with a moderate yield. However, for obtaining α-anomers *via* $SnCl_4$-mediated glycosylation, the optimized reaction time for lactosides and maltosides dramatically differed: 18 h *vs.* 3 d, respectively. Detailed synthesis and purification procedures and associated $^1$H NMR spectra are in the SI (Fig. S1–S20). For the synthesis of Guerbet cellobiosides, please refer to our previous publication.[54]

To characterize the thermotropic self-assembly of dry glycolipids, all compounds were lyophilized for at least four days and subsequently stored in the glovebox under nitrogen. Compound purity and dryness were verified by elemental analysis (SI, content IV). Herein, the compounds are referred to as $x$-Y-$C_zC_{z-4}$ where $x$ refers to anomeric stereochemistry (α/β), Y denotes the disaccharide unit (Cel for cellobiose, Mal for maltose, Lac for lactose) and $z$ = 6–14 represents the longer alkyl chain length of the Guerbet alcohol.

### Characterization of glycolipid phase behavior

The thermotropic phase behavior was examined *via* DSC and POM to identify the temperature range for self-assembly; for detailed thermal characterization, see SI Section IX. Maltosides begin forming LC phases at $T \geq 60$ °C, depending on chain length (Table S2 and Fig. S22a) whereas lactosides exhibited significantly higher melting temperatures (113–178 °C) compared to both cellobiosides ($T \geq 85$ °C) and maltosides.[54] Beyond the melting endotherm (Fig. S21–22b), another high-temperature endothermic peak, assigned to the thermotropic LC clearing temperature (order-to-disorder transition temperature, $T_{ODT}$; Fig. S21), is evident for most glycolipids. Generally, $T_{ODT}$ increases monotonically with Guerbet chain length (Fig. S22b), following a trend similar to that reported in other glycolipids.[46,54] Overall, changing the glycolipid head from cellobiose to lactose and maltose significantly alters the LC temperature window, especially the melting temperature ($T_m$). Maltosides exhibit the lowest $T_m$, whereas lactosides show the highest (Table S2). This observation suggests that subsequent differences in packing behavior could similarly result from subtle variations in glycolipid stereochemistry.

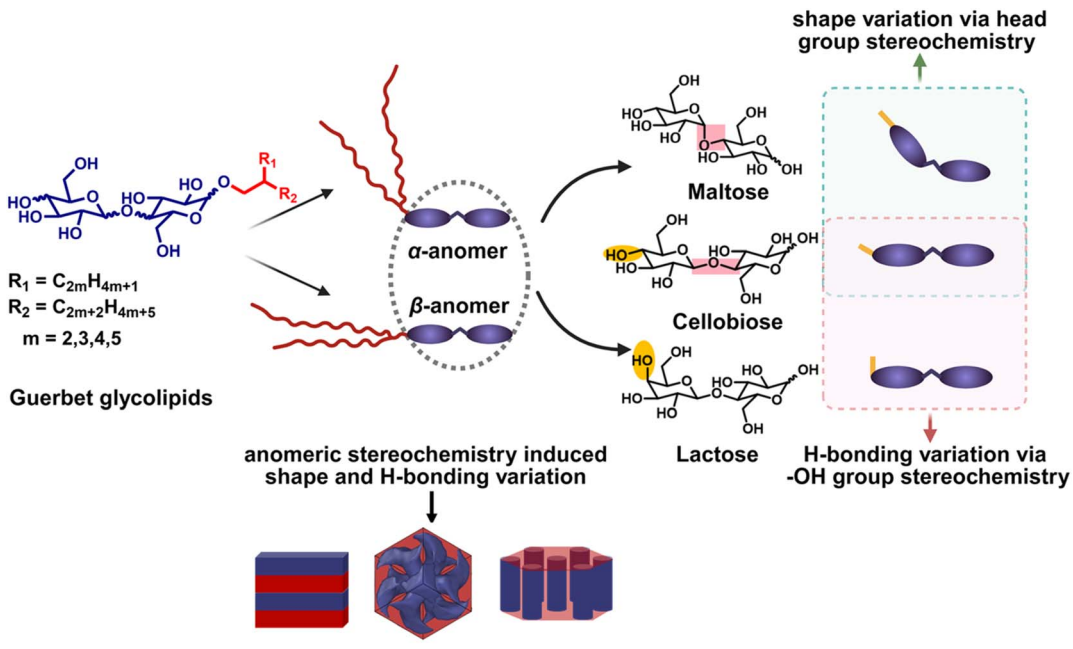


Fig. 1 Design of disaccharide glycolipids to systematically examine the impact of molecular shape and hydrogen bonding on thermotropic self-assembly. The headgroup shape is similar for cellobiose and lactose but differs for maltose-based glycolipids. The yellow line corresponds to the direction of the C4′ hydroxyl, which is the same for cellobiose and maltose but differs for lactose; the pink box indicates a change in molecular shape due to a change in the glycosidic bond position between the monosaccharide units, which is an α(1–4) glycosidic bond for maltose and a β(1–4) glycosidic bond for cellobiose and lactose.

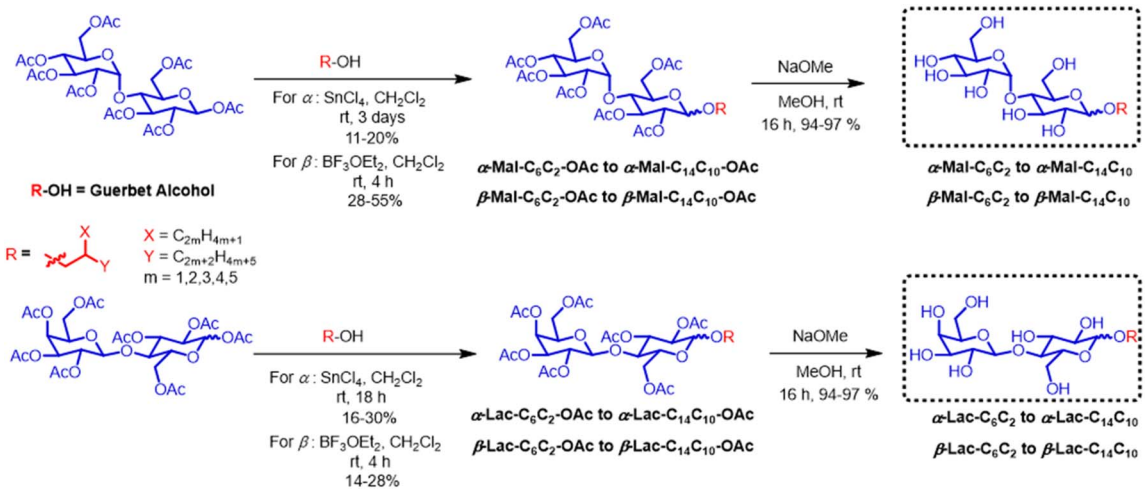


Scheme 1 Lewis acid-mediated glycosylation of Guerbet α- and β-lactosides and maltosides.

### No non-lamellar phases in α-maltosides

Variable temperature SAXS was then used to identify thermotropic ordering in Guerbet lactosides and maltosides. All maltosides started forming LC phases at $60 \leq T \leq 85$ °C (Table S2), except for the shortest alkyl chain ($-C_6C_2$) for which no LC phase was detected for the α-anomer (Fig. S25a). Unlike in α-cellobiosides,[54] α-maltosides form only LAM phases for all other Guerbet tails ($-C_8C_4$ to $-C_{14}C_{10}$) (Fig. 2a and S25–S29). For Guerbet α-maltosides, LAM phases were identified *via* POM and the appearance of SAXS peaks corresponding to the (100) and (200) reflections (Fig. 2a, S26–S29 and S30b). Notably, the bent shape of the α-maltosides leads to consistently smaller domain spacings *vs.* analogous β-anomers forming the same phase (Table S3).

In contrast, increasing the Guerbet chain length yields non-lamellar phases in β-maltosides. As in Guerbet cellobiosides,[54] LAM forms in β-Mal-$C_6C_2$ (Fig. S25b and S30a); however, unlike β-cellobiosides, LAM is also observed for β-maltosides with $-C_8C_4$ and $-C_{10}C_6$ tails for the entire LC window (Fig. 2b and S26–S27). Upon melting, β-Mal-$C_{12}C_8$ initially forms LAM (Fig. S28b) displaying birefringence in POM; with further temperature elevation, the birefringence disappears in favor of a non-birefringent isotropic viscous liquid (Fig. S30d), typically a cubic phase. A small endothermic peak corresponding to this order-to-order phase transition (OOT, Fig. S21b) is also observed *via* DSC near 118 °C. Although during heating, the 1D SAXS trace contains low-intensity peaks (Fig. 2b), the peaks become more pronounced upon cooling (Fig. S31). The peak locations at $(q/q^*)^2 = 6$, 8, 14, 16, 20, and 22 correspond to the (211), (220), (321), (400), (420), and (332) reflections of a thermotropic DG phase with $Ia\bar{3}d$ space group symmetry. From POM, DSC, and SAXS, the thermal stability of the DG formed by β-Mal–$C_{12}C_8$ is $\Delta T = 69$ °C, exceeding that of α-Cel–$C_{12}C_8$ ($\Delta T = 47$ °C).[54] Similar to α-Cel–$C_{12}C_8$, a highly textured ("spotty") 2D SAXS pattern is observed for β-Mal–$C_{12}C_8$, indicating long-range translational order and a large grain size (Fig. S32).

When the Guerbet tail length is increased to $-C_{14}C_{10}$, β-maltoside immediately forms a DG phase upon melting (Fig. S29b). The DG unit cell parameter increases from 83.7 to 94.9 Å upon increasing the tail length from $-C_{12}C_8$ to $-C_{14}C_{10}$ (Table S3). Further temperature elevation to 145 °C results in an OOT to HEX (Fig. 2b and S29b), with characteristic scattering peaks located at $(q/q^*)^2 = 1$, 3, 4,… and a corresponding endothermic peak in the DSC trace (Fig. S21b). POM confirms a DG thermal stability of 30 °C in β-Mal–$C_{14}C_{10}$, much lower than α-Cel–$C_{14}C_{10}$ ($\Delta T = 78$ °C). Nevertheless, both molecules with a single topological kink – β-maltosides (headgroup kink) and α-cellobiosides (anomeric kink) – form stable DG phases at two different tail lengths. Conversely, molecules with two topological kinks (α-maltosides) fail to form DG, and those with no kink in topology (β-cellobioside) form DG at only one tail length. These proposed changes in topology are confirmed *via* MD simulations and discussed further below.

### Inability of α-lactosides to stabilize DG

In contrast to maltosides, systematically increasing the Guerbet chain length directs lactoside self-assembly toward non-lamellar phases for both anomers (Fig. 2c and d). However, for all lactosides, the LC temperature window is diminished due to the high $T_m$ (Table S2 and Fig. S33–S37). Thermotropic LAM phases, indicated by peaks at $(q/q^*)^2 = 1$, 4, … are identified at chain lengths of $-C_8C_4$ to $-C_{12}C_8$ for α-anomers and up to $-C_{10}C_6$ for β-anomers (Fig. 2c, d and S33–S36). With short $-C_6C_2$ tails, both anomers melt directly to isotropic liquids at exceptionally high temperatures (Fig. S33). This crystalline stability for short tails ($-C_6C_2$) is disrupted when the Guerbet chain length is increased, leading to lower $T_m$ and LC ordering.

The thermotropic phase behavior for the two anomers diverges at a tail length of $-C_{12}C_8$. A SmA-type LAM was detected by POM for α-Lac-$C_{12}C_8$ (Fig. S36a and S38) between 148 and 175 °C. In contrast, β-Lac-$C_{12}C_8$ melts at 124 °C to form DG, which persists for a temperature window of $\Delta T = 64$ °C (124–188 °C). The corresponding DG lattice parameter is 84.8 Å – higher

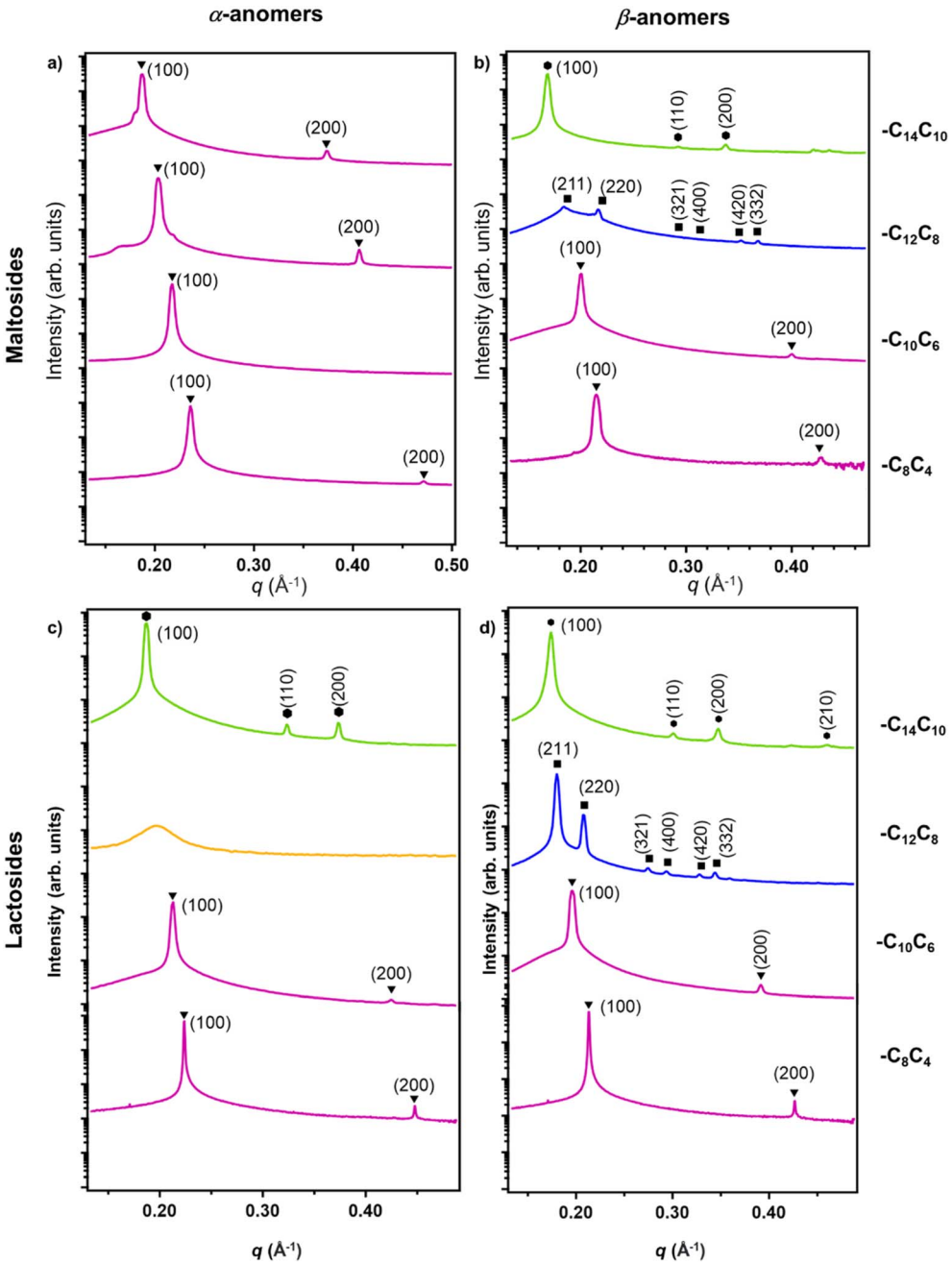


Fig. 2 Azimuthally integrated SAXS intensities for (a) α-maltosides at 115 °C, (b) β-maltosides at 145 °C, (c) α-lactosides at 175 ± 5 °C and (d) β-lactosides at 145 °C with different Guerbet tails, shifted vertically for clarity. Filled triangle, square, and hexagon markers indicate calculated peak positions for LAM, DG, and HEX, respectively. Phase behavior from SAXS was confirmed with POM; α-Lac-$C_{12}C_8$ forms LAM from 148–175 °C (Figure S38).

than for both α-Cel-$C_{12}C_8$ (80.7 Å) and β-Mal-$C_{12}C_8$ (83.7 Å) (Table S4). This larger lattice parameter in β-Lac-$C_{12}C_8$, despite equivalent tail length, is likely due to the more planar conformation of this molecule *vs.* α-Cel-$C_{12}C_8$ (bend at anomeric position) and β-Mal-$C_{12}C_8$ (bend in headgroup).

Upon lengthening the tail from $-C_{12}C_8$ to $-C_{14}C_{10}$, both anomers form stable HEX across the LC window (Fig. 2c, d and S37); this behavior is expected based on the increase in hydrophobic volume. Interestingly, for α-Lac-$C_{14}C_{10}$, a narrow range of coexisting DG/HEX appears upon melting and reappears upon cooling (Fig. S37a and S39), suggesting that DG may have a low thermal stability that is undetectable within the 30 °C SAXS temperature interval. Notably, the similarly shaped α-cellobioside exhibits wide DG thermal stability at this tail length, suggesting that the stereochemistry change of the C4′ hydroxyl group may significantly alter key hydrogen bonding motifs that stabilize DG.[50] Overall, the lactoside phase behavior demonstrates that a single kink in molecular topology alone is insufficient to produce highly-stable DG.

### Comparative analysis of phase behavior in disaccharide-based Guerbet glycolipids

These results for disaccharide Guerbet glycolipids highlight the combined effect of sugar stereochemistry, anomeric configuration and headgroup hydrogen bonding on thermotropic self-assembly into network phases. Based on DSC, SAXS, and POM, the tail length- and temperature-dependent phase behaviors of all lactosides, maltosides and cellobiosides are summarized in Fig. 3a and b within the temperature range of $T = 25$–$240$ °C.

Generally, Guerbet glycolipids form non-lamellar phases with increasing chain length, except for α-maltosides which only form LAM (Fig. 3a and b). For each pair of glycolipid anomers, β-anomers consistently form non-lamellar phases at shorter chain lengths *versus* α-anomers. Zahid *et al.* saw a similar trend in glucopyranoside and galactopyranoside glycolipids with a $-C_{10}C_6$ Guerbet tail.[47] The overall phase diagram (Fig. 3a and b) indicates that the order-to-disorder transition temperatures ($T_{ODT}$) are generally higher for β-*vs.* α-anomers, as in other glycolipids.[21,48,54] A clear trend in $T_{ODT}$ is also apparent: $T_{ODT}$ generally increases as chain length increases from $-C_8C_4$ to $-C_{14}C_{10}$, likely due to enhanced van der Waals interactions. One exception is α-Mal-$C_{14}C_{10}$, where a significant drop in $T_{ODT}$ occurs between $-C_{12}C_8$ and $-C_{14}C_{10}$ (Table S2 and Fig. S22b). A distinct trend is also observed in the melting temperatures ($T_m$), where lactosides consistently exhibit higher $T_m$ than their homologous cellobiosides[54] and maltosides (Table S2 and Fig. S22a).

A comparison of LAM *d*-spacings reveals that α-glycosides consistently form smaller domain spacings than the analogous β-glycosides with the same headgroup and tail length (Tables S3 and S4), due to the bent molecular topology imparted by the anomeric stereochemistry.[54] When comparing glycolipids with the same anomeric configuration and Guerbet chain that form LAM phases at the same temperature, maltosides consistently adopt the smallest *d*-spacings. For example, in α-$C_8C_4$ glycosides at 85 °C, the lamellar *d*-spacing is 26.1 Å *vs.* 28.1 Å for the maltoside *vs.* cellobioside (Table S3);[54] similarly, β-$C_{10}C_6$ maltoside forms bilayers of 31.2 Å *d*-spacing at 145 °C (Table S3) *vs.* a *d*-spacing of 32.1 Å in the corresponding lactoside (Table S4). However, POM images during heating and cooling for all $-C_8C_4$

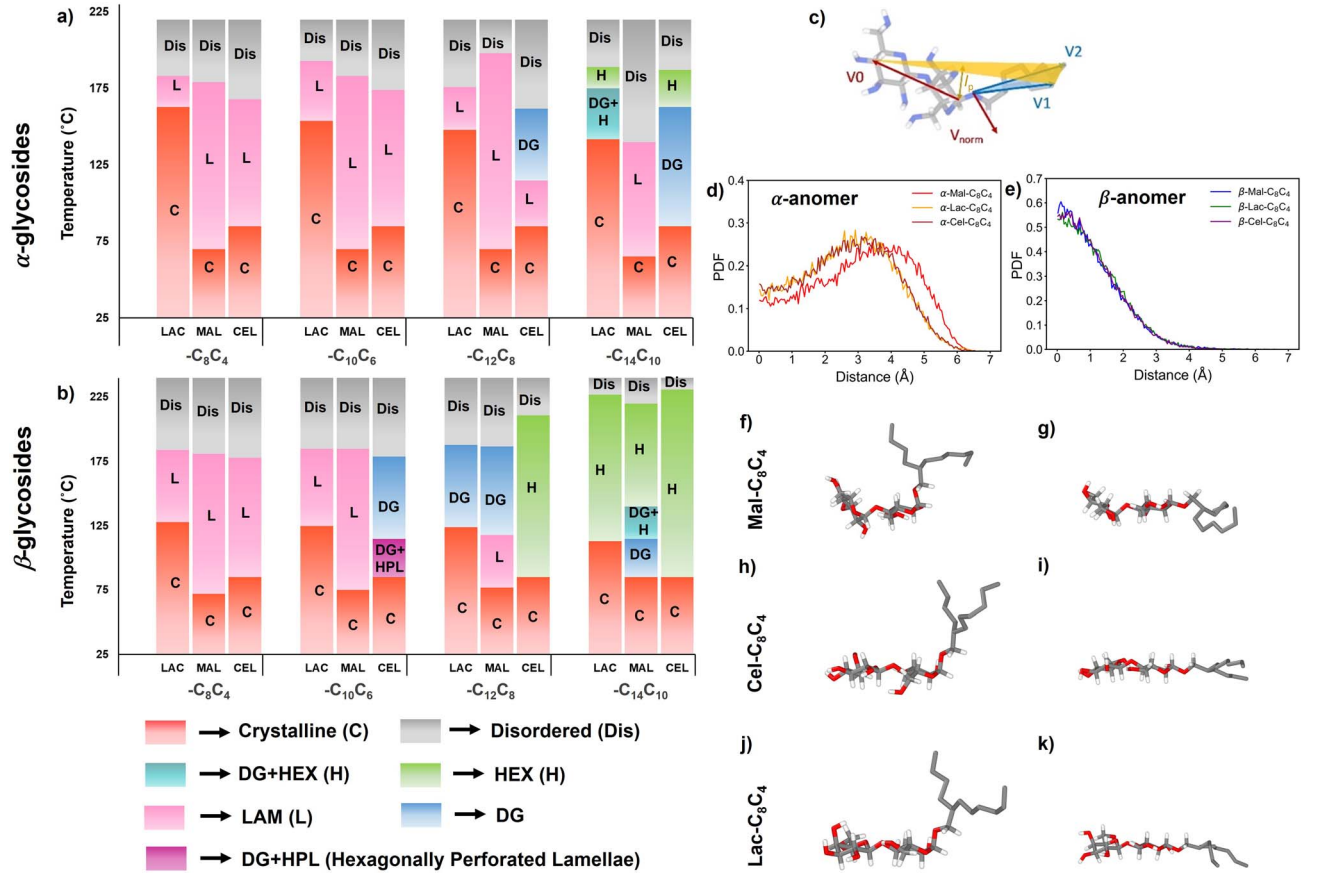


Fig. 3 Phase behavior on heating and cooling of (a) α-glycosides and (b) β-glycosides with tails from $-C_8C_4$ to $-C_{14}C_{10}$ from 25–240 °C, *via* SAXS, POM and DSC. For DG-forming molecules, the phase behavior during the first heating is shown, as DG does not revert to other phases upon cooling within the experimental time frame. (c) Sketch of plane formed by the distal carbon atoms of the sugar and tail groups (yellow, "glycolipid plane") and by the ether linker and tail ends (blue "tail plane"). Probability distribution of the distance $l_p$ between the C1 atom and glycolipid plane for (d) α-glycosides, (e) β-glycosides. Representative molecular conformations of $C_8C_4$-glycosides in LAM structures obtained from MD simulations: (f) α- and (g) β-Mal; (h) α- and (i) β-Cel; (j) α- and (k) β-Lac.

glycosides reveal similar focal conic textures, characteristic of lamellar SmA assemblies with no net in-plane orientational order (Fig. S40).

### Molecular shape and bilayer packing of the glycolipids by MD simulation

To confirm the proposed molecular shapes and gain a deeper understanding of shape-dependent molecular packing and hydrogen bonding in Guerbet glycolipids, atomistic molecular dynamics (MD) simulations were carried out on LAM-forming glycolipids with $-C_8C_4$ tails. The systems were allowed to equilibrate for at least 1 μs, and the production period used for analysis consisted of 200 ns, as done previously.[54] To ensure that anomers of the same headgroup each formed LAM, MD simulations on Mal-$C_8C_4$, Cel-$C_8C_4$, and Lac-$C_8C_4$ were done at 360 K, 390 K, and 420 K, respectively; no single temperature could be used across all six molecules, given the differences in $T_m$. For simulation details and information on additional simulations, see SI (Fig. S41–S48).

MD simulations accurately replicate experimental results, confirming that α-anomers have smaller LAM *d*-spacings than β-anomers (Fig. S41). Generally, α-anomers form bent "boomerang" shapes with shorter head-to-tail distances, while β-anomers are more planar and rod-like (Fig. 3f–k). This difference in molecular shape can be quantified by the probability distributions of the distance $l_p$ between the C1 atom and the plane formed by the distal carbon atoms of the sugar and tail groups ("glycolipid plane", Fig. 3c–e). The most probable $l_p$ for β-anomers is zero but ranges from 2 to 5 Å for α-anomers. Consistent with prior results,[54] heat maps of conformational populations reveal that α-anomers adopt a broad range of conformations upon packing, while most β-anomers preferentially align their headgroup coplanar with the tail (Fig. S42).

An additional kink in the molecular structure is seen for maltosides (Fig. 3f and g), which adopt a wedge-shaped headgroup due to the α(1 → 4) glycosidic bond between sugar units, in contrast to the β(1 → 4) bond in cellobiose and lactose. Distance distributions between distal carbon atoms of the sugar and tail (Fig. S43) confirm that maltosides exhibit the shortest head-to-tail distances, consistent with the bent headgroup shape and the small experimental *d*-spacings. For α-maltosides, kinks in both the headgroup and at the anomeric position result in the largest shape irregularities and smallest *d*-spacings among glycosides (Fig. 3f, Tables S3 and S4). This behavior is exemplified by the $l_p$ probability distribution for α-maltoside, which shows most probable conformations between 3 Å ≤ $l_p$ ≤ 5 Å compared to 2 Å ≤ $l_p$ ≤ 4 Å for other α-glycosides (Fig. 3d). Consequently, α-maltosides exhibit nearly random headgroup orientations in the bilayer (Fig. S46g), whereas headgroups of α-cellobiosides and α-lactosides are more ordered, with most probable tilt angle relative to the bilayer normal being ∼44° and ∼50°, respectively (Fig. S46h and i). Heat maps also confirm that α-maltosides have the highest population of folded-tail conformations (Fig. S44 a–c) and exhibit greater overlap between the headgroups and tails (Fig. S46a). This highly irregular, inefficient packing likely hinders formation and stabilization of non-lamellar phases in α-maltosides (Fig. 4) and weakens LAM phase stability at longer chain lengths ($-C_{14}C_{10}$), lowering $T_{ODT}$.

In contrast, β-maltosides that lack a kink at the anomeric position exhibit less shape irregularity and better packing efficiency (Fig. 3g, S46a and b). Of all β-glycosides, β-maltosides produce the highest DG stability (69 °C, $-C_{12}C_8$) compared to cellobiosides (64 °C, $-C_{10}C_6$)[54] and lactosides (64 °C, $-C_{12}C_8$); a stable DG phase was also formed by a second β-maltoside ($-C_{14}C_{10}$). Interestingly, these same β-maltosides adopt a higher tilt angle (∼50°) relative to the bilayer normal (*vs.* ∼34° in β-cellobiosides, ∼25° in β-lactosides) in MD simulations, leading to greater head-tail overlap and a less coplanar structure than the other two β-glycosides (Fig. S46). The lower headgroup densities and higher head-tail overlap in β-maltosides is reminiscent of the packing in α-*vs.* β-cellobioside bilayers, where α-anomers form higher stability DG at longer tail lengths than β-anomers.[54] Conversely, higher headgroup densities for β-cellobiosides and β-lactosides and limited head–tail overlap (Fig. S46d and f) may cause their higher $T_{ODT}$.

Headgroup tilting from the bilayer normal is often found as a means to relieve packing frustration in lipid bilayers.[21,54–56] These higher tilt angles may enable β-maltosides to accommodate larger hydrophobic volumes when packed into bilayers, as an increased surface area per chain could relieve the need for distorting the interface as tail volume increases.[57,58] As such, this higher tilt angle may delay DG formation to longer chain lengths in β-maltosides ($-C_{12}C_8$, $-C_{14}C_{10}$) *vs.* β-cellobiosides ($-C_{10}C_6$) or β-lactosides ($-C_{12}C_8$). A similar trend was observed in our prior work, where a higher tilt angle in α- *vs.* β-cellobioside bilayers at shorter tail lengths ($-C_8C_4$) was associated with DG formation at longer chain lengths for α-anomers.[54] Notably, among glycolipids examined here, DG thermal stability at longer tail lengths was greatest for α-cellobiosides (78 °C) and β-maltosides (69 °C), which exhibited comparable tilt angles when packed into bilayers at shorter tail lengths ($-C_8C_4$); for the rest of the DG-forming molecules, the tilt angle was much lower. Thus the higher DG stability in β-$C_{12}C_8$ maltosides *vs.* β-cellobiosides and lactosides may be correlated with the higher bilayer tilt angle, lower headgroup densities, and higher degree of head and tail overlap – features also observed in α-cellobiosides with enhanced DG stability.[54]

### Factors influencing DG formation and stabilization in glycolipids

The role of headgroup hydrogen bonding between glycolipids in maintaining lipid bilayer stability and membrane function is well established;[59–61] less regular H-bonding between headgroups in packed cellobioside bilayers (short tails) was also correlated with higher DG stability at longer tail lengths in α-*vs.* β-cellobiosides.[54] Thus, to better understand what molecular features may enable planar packings to destabilize in favor of stable DG with increasing tail length, heat maps of hydrogen bonding between headgroups of each glycoside were generated from MD simulations of packed bilayers with $-C_8C_4$ tails (Fig. S47 and S48; see Fig. S49 for description of hydroxyl group

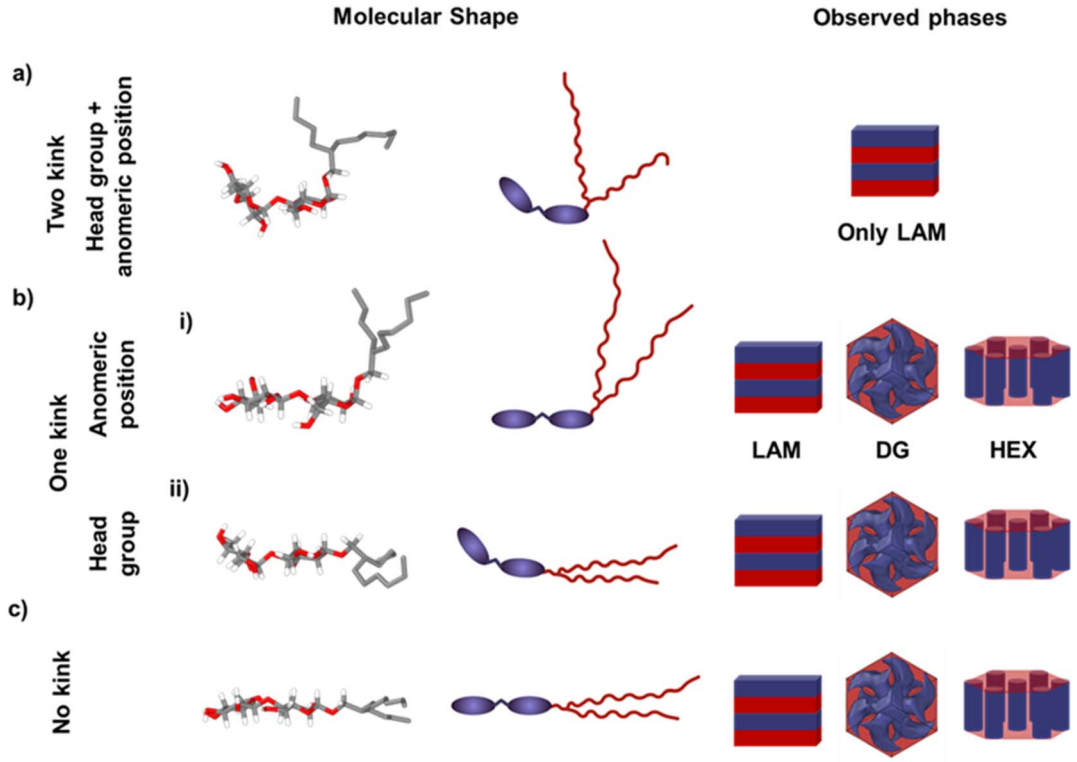


Fig. 4 Overall phase behavior of the glycolipids based on number of kinks present in their shape (a) α-maltosides with two kinks (at the head group and anomeric position) showing only LAM phase formation, (b) one kink either at (i) anomeric position (α-cellobiosides/lactosides), (ii) or at head group (β-maltosides) producing LAM, DG and HEX phases, (c) no kink in the molecular shape displaying LAM, DG and HEX phases.

numbering with respect to sugar carbons). Although generated at different temperatures based on headgroup, the heat maps identify the role of specific headgroup hydroxyls in forming intra- or interlayer H-bonds. Here, "intra-" and "inter-layer" H-bonding specifies H-bond between neighboring sugar headgroups present in the lateral and perpendicular direction to the bilayer normal, respectively (Fig. S50). Notably, H-bond heat map values for specific donor and acceptor sites are only compared after normalizing by the total intra- or inter-layer H-bonding interactions at that temperature (Table 1).

Despite differences in temperature, headgroup, and anomeric stereochemistry, all molecules forming DG at longer tail lengths ($-C_{10}C_6$ and above) shared similar inter-layer H-bonding motifs in packed bilayers with $-C_8C_4$ tails. DG is stable in four of the six glycosides: β-glycosides with all three headgroups, and α-cellobiosides. DG never forms in α-maltoside, and forms only while coexisting with HEX in α-lactoside. Inspecting these heat maps reveals a clear correlation between DG stability and substantial inter-layer H-bonding between the outer sugar hydroxyl groups, *i.e.*, those farthest from the tail connected to the C3′ and C4′ carbons (Fig. S47 and S48). In fact, the four glycolipid anomers that stabilize DG phases at longer tail lengths have between 17% and 23% of their total inter-layer H-bonding localized to these two hydroxyl groups (Table 1). However, when this relative interlayer H-bonding fraction drops below 0.17, DG phase at longer tail lengths is no longer stable. In α-lactoside, which forms DG coexisting with HEX for a small window, only 12% of the total inter-layer H-bonds occur between the C3′ and C4′ hydroxyl groups; in α-maltosides that never form DG, this value is 9%.

Table 1 Summary of inter-layer H-bonds from MD simulations on glycolipids with $-C_8C_4$ tails in packed bilayers (Fig. S47 and S48), including total inter-layer bonds (temperature-dependent) and fraction of inter-layer bonds localized to C3′ and C4′ hydroxyl groups (normalized). Molecules are presented in order of increasing (relative) inter-layer H-bonding between C3′ and C4′ hydroxyls, which is correlated with DG stabilization at longer tail lengths

| Glycolipid | $T$ (K) | Total inter-layer H-bonds | Fraction of inter-layer bonds by C3′, C4′–OH | DG stabilization at longer tail lengths |
|---|---|---|---|---|
| α-Mal | 360 | 1.38 | 0.09 | No DG |
| α-Lac | 420 | 1.14 | 0.12 | DG/HEX coexistence: $-C_{14}C_{10}$ (30 °C) |
| α-Cel | 390 | 1.44 | 0.17 | DG: $-C_{12}C_8$ (47 °C), $-C_{14}C_{10}$ (78 °C) |
| β-Mal | 360 | 1.43 | 0.17 | DG: $-C_{12}C_8$ (69 °C), $-C_{14}C_{10}$ (30 °C) |
| β-Lac | 420 | 1.42 | 0.23 | DG: $-C_{12}C_8$ (64 °C) |
| β-Cel | 390 | 1.62 | 0.23 | DG: $-C_{10}C_6$ (64 °C) |

Notably, the two systems in which 17% of interlayer H-bonding is concentrated at the C3′ and C4′ hydroxyls also exhibit the highest DG thermal stabilities and form DG phases at two tail lengths, suggesting that this value is near to optimal H-bonding. In contrast, when this value increases to 23%, DG still forms, but the thermal stability is lower. This higher inter-layer hydrogen bonding occurs in molecules without a topological kink and may be a consequence of their more uniform packing, suggesting that the DG stability may be lowered because this planar packing is more difficult to destabilize. Given that C3′ and C4′ hydroxyl groups are highly likely to engage in inter-layer hydrogen bonding (and the C4′ –OH stereochemistry is altered between cellobiose and lactose), the analysis focused on these positions; however, the trend still holds if inter-layer H-bonds are considered between a broader set of outer hydroxyls (C3′, C4′, C6′). While this correlation may not be causal, subsequent DG stability cannot be explained by total inter-layer H-bonding (Table 1) or intra-layer H-bonding patterns (Fig. S47 and S48). Overall, systems in which the 17% of the interlayer hydrogen bonding is located at the outer hydroxyl groups (C3′ and C4′) were found to produce optimal DG stability. When this fraction of interlayer H-bonding is reduced below 12% or increased above 23%, DG stability is either lost or lowered.

### DG stabilization in β-maltosides and α-cellobiosides: role of molecular shape

Across glycolipids, β-maltosides and α-cellobiosides produce the highest DG stabilization: both form DG at two tail lengths (–$C_{12}C_8$ and –$C_{14}C_{10}$) over a similar total temperature window. Beyond sharing the same fraction of inter-layer bonds by C3′and C4′ hydroxyl groups, these molecules also exhibit a pronounced topological kink (Fig. 3g and h). However, the kink in the β-maltoside occurs in the headgroup (*i.e.*, shorter distance) than that for α-cellobioside which occurs between the headgroup and tail. Interestingly, with shorter –$C_{12}C_8$ tails, DG thermal stability for β-maltoside (69 °C) is higher than for α-cellobioside (47 °C). The opposite is true for longer –$C_{14}C_{10}$ tails, where DG is stable for 30 °C (β-maltoside) *vs.* 78 °C (α-cellobioside). As such, the relative kink position along the molecule is similar for β-Mal-$C_{12}C_8$ and α-Cel-$C_{14}C_{10}$. This result suggests that while shape irregularity and a proper balance of inter-layer H-bonds are essential for enhancing DG thermal stability, the kink position also matters (Fig. 5), in agreement with prior work showing that DG stability is influenced by the kink position in the tail.[62] In addition to DG formation, the overall phase behavior of the glycosides, categorized according to the number and position of kinks, is summarized in Fig. 4.

### Role of headgroup hydrogen bonding on tail length for DG formation

Despite similar shapes, β-lactosides form DG with longer tails (–$C_{12}C_8$) than β-cellobiosides (–$C_{10}C_6$). In packed bilayers, the C4′ hydroxyl stereochemistry in β-lactoside promotes formation of intra-rather than inter-layer H-bonds (Fig. S48). Consequently, a more uniform distribution and slightly higher magnitude of intra-layer H-bonds are observed in the headgroup region of β-lactosides *vs.* β-cellobiosides (despite higher simulation temperatures). Lipids with galactose headgroups (outer sugar ring of lactose) have shown stronger headgroup hydrogen bonding compared to those with glucose headgroups (outer sugar ring of cellobiose).[63] As such, the headgroup environment in β-lactosides is likely more constrained – mitigating the average headgroup tilt within the bilayer (∼25° *vs.* ∼34° in β-cellobiosides) and thereby necessitating longer tail lengths to destabilize the bilayer toward negative Gaussian curvature DG phases. The higher $T_m$ in lactosides is consistent with a more constrained headgroup due to the C4′ hydroxyl orientation – and increased intermolecular cohesion due to more regular tail packing, as seen in lactosylceramide lipids with saturated acyl chains.[64] Similar headgroup H-bond-driven changes in aggregation were also seen in phenyl- and methyl-substituted glucose and galactose molecules.[65] Conversely, the tail length for optimal DG stability in β-maltosides appears to depend more on kink position, as the shape irregularity allows these headgroups to tilt more freely upon packing (∼50°).

In contrast, α-lactosides do not form stable DG despite the similar shape to α-cellobiosides; here, DG/HEX coexist for ∼30 °C for –$C_{14}C_{10}$ tails. Here, the substantial headgroup tilt in the bilayer (∼50°), paired with the change in orientation of the C4′ hydroxyl, drastically reduces total interlayer H-bonds *vs.* other glycosides (Table 1). The fraction of inter-layer H-bonds between C3′, C4′ hydroxyls is also reduced by ∼40% *vs.* the α-cellobioside that forms a highly stable DG. However, coexisting DG forms in α-lactoside despite very weak total inter-layer H-bonding (Table 1), further supporting that specific H-bonding motifs play a key role in stabilizing DG (Fig. 5).

### Role of molecular shape *vs.* headgroup hydrogen bonding on forming and stabilizing DG

This extensive dataset confirms that both molecular shape irregularity and specific headgroup hydrogen bonding motifs are critical for forming and stabilizing DG phases in disaccharide Guerbet glycolipids, after reaching a hydrophobic volume fraction of 0.48.[54] The highest DG thermal stability occurs in two glycosides (β-maltosides; $\Delta T_{DG} = 69$ °C, α-cellobiosides; $\Delta T_{DG} = 78$ °C) with a topological kink and moderate (∼17%) localization of inter-layer H-bonds to the C3′ and C4′ hydroxyls. The topological kink leads to a wide range of molecular conformations, significant overlap between headgroup and tails upon packing (Fig. S44 and S46), and a high headgroup tilt angle in the bilayer (∼50°) – a feature typically preceding DG formation.[66–69] However, shape irregularity is not enough: α-lactosides with a similar shape and headgroup tilt but lacking these specific H-bonding motifs fail to produce stable DG. Further, excessive shape irregularity is detrimental to DG formation. In α-maltosides, multiple kinks cause inefficient packing and nearly random headgroup orientations, such that critical H-bonds between C3′ and C4′ hydroxyls are lost.

The kink position also influences DG stability.[62] The most stable DG in β-maltosides and α-cellobiosides share a similar kink position; however, defining an optimal kink position is

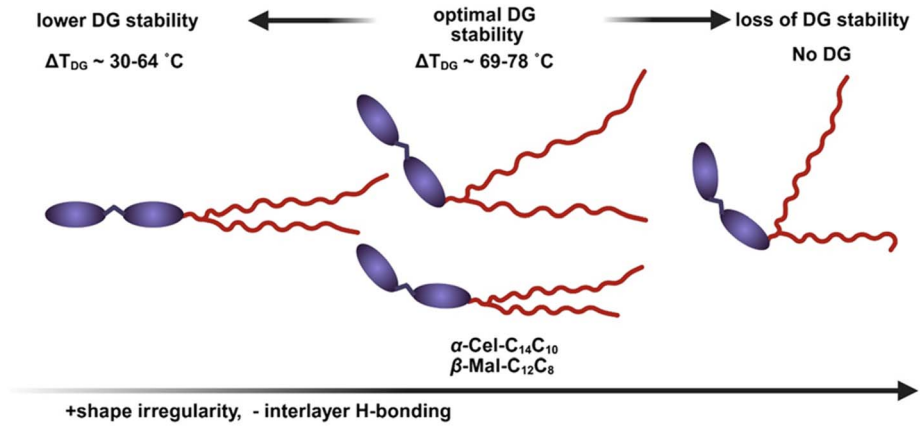


Fig. 5 Schematic representation of the factors responsible for DG stabilization in glycolipids. Optimal DG stability in Guerbet glycolipids were obtained with one kink in the molecular shape, for α-cellobioside (78 °C, $-C_{14}C_{10}$) and β-maltosides (69 °C, $-C_{12}C_8$). DG stability is reduced with flat shaped glycolipids (no kink in the molecular shape) for β-cellobiosides (64 °C, $-C_{10}C_6$) and β-lactosides (64 °C, $-C_{12}C_8$). DG stability is lost in glycolipids with irregular shape (α-maltosides; two kinks in the molecular shape) or reduced interlayer hydrogen bonding (α-lactosides).

difficult given the different tail lengths and wide range of average molecular conformations. As a rough estimate, here the "kink distance" (*i.e.*, distance from outer headgroup –OH to kink) is a significant fraction of the tail length, but is not at the center of the molecule. For example, in α-Cel-$C_{14}C_{10}$, the kink occurs at the anomeric position ("distance" is the disaccharide length, ~1 nm), which is shorter than either $-C_{14}C_{10}$ tail branch assuming a 1.54 Å C–C single bond distance. When the kink is closer to the molecule center (α-Cel-$C_{12}C_8$), DG stability is lower. For β-Mal-$C_{12}C_8$ with a kink in the headgroup, the kink distance is also shorter than either tail branch. However, when the kink distance is very short (β-Mal-$C_{14}C_{10}$), DG stability also decreases.

In contrast, for β-glycolipids that assume more planar topologies (β-cellobioside, β-lactoside), the shape irregularity imparted by the Guerbet tail is sufficient for DG to form at moderate tail lengths ($-C_{10}C_6$, $-C_{12}C_8$). Here, DG emerges at only one tail length and thermal stability is lower than for best-performing molecules with a topological kink. Bilayer packing is also more regular than for kinked molecules, and ~23% of all inter-layer H-bonds are localized to those between C3′ and C4′ hydroxyls. These bilayers (Fig. S46d and f) are also associated with single average molecular conformation, low headgroup tilt upon packing (≤34°), and stronger total inter-layer and intra-layer H-bonds than for analogous α-anomers, making destabilization difficult and likely limiting DG stability. The tail length at which DG forms is related in part to headgroup constraints, where stronger and more uniform intra-layer H-bonds delay DG formation to longer tail lengths.

In totality, this evidence suggests that shape irregularity from both a branched tail and single topological kink is optimal to form stable DG, but only if sufficiently strong H-bonds can stabilize the packing across regions of changing Gaussian curvature. Among all glycolipids, α-$C_{14}C_{10}$ cellobioside appears to best balance molecular shape and hydrogen bonding, yielding the most stable DG. These findings underscore that the design of DG-forming glycolipid amphiphiles hinges on understanding the interplay between molecular shape, head group hydrogen bonding and hydrophilic/hydrophobic balance, which collectively influence molecular packing. A single kink with moderate (~17%) localization of inter-layer H-bonds to the C3′ and C4′ hydroxyls groups (α-cellobiosides, β-maltosides) promotes DG with two chain lengths ($-C_{12}C_8$, $-C_{14}C_{10}$) and maximal stability ($\Delta T_{DG}$ = 69–78 °C). Even without a kink, DG can be stabilized, although with reduced thermal stability ($\Delta T_{DG}$ = 64 °C), by the shape irregularity from Guerbet tails combined with a slightly elevated inter-layer H bonds (~23%). However, higher shape irregularity by the presence of two kinks (α-maltosides) or a significant loss of inter-layer H bonds (≤12%) resulted in loss of DG stability (α-maltosides, α-lactosides).

## Conclusion

Experimental and molecular dynamics studies of anomerically-pure Guerbet glycosides with cellobiose, lactose, and maltose headgroups and varying alkyl tail lengths reveal that, in addition to the appropriate hydrophilic/hydrophobic balance, amphiphile shape and headgroup inter-layer hydrogen bonds critically influence self-assembly into network phases. Despite having a similar hydrophilic/hydrophobic balance, DG phase emergence is delayed to higher tail length in systems with a topological bend (α-anomers, β-maltosides). The kink in the molecular shape increases the surface area per lipid chain, which helps accommodate larger tail volumes and thus pushes DG formation towards longer tail lengths. The molecular flexibility that alleviates packing frustration also contributes to an enhanced DG thermal stability window as witnessed for β-Mal-$C_{12}C_8$ ($\Delta T_{DG}$ = 69 °C), α-Cel-$C_{14}C_{10}$ ($\Delta T_{DG}$ = 78 °C). However, this effect is influenced by the kink position relative to the molecular length, evidenced by the DG stability of α-cellobiosides (α-Cel-$C_{12}C_8$; $\Delta T_{DG}$ = 47 °C, α-Cel-$C_{14}C_{10}$; $\Delta T_{DG}$ = 78 °C) *vs.* β-maltosides (β-Mal-$C_{12}C_8$; $\Delta T_{DG}$ = 69 °C, β-Mal-$C_{14}C_{10}$; $\Delta T_{DG}$ = 30 °C). While the most stable DG phases are formed by

molecules with a topological bend, the shape irregularity imparted by the Guerbet tail is also sufficient to enable DG formation in β-cellobiosides ($\Delta T_{DG}$ = 64 °C) and β-lactosides ($\Delta T_{DG}$ = 64 °C) with no topological kink. However, extreme shape irregularity, *i.e.*, introducing two kinks in shape (α-maltosides), is detrimental to DG formation.

In addition to optimum shape irregularity, balancing the inter- and intra-layer hydrogen bonding in the headgroup area is also pivotal in forming and stabilizing DG. Despite differences in temperature, headgroup, and anomeric stereochemistry, all molecules that form DG at longer tail lengths ($-C_{10}C_6$ and above) shared similar inter-layer hydrogen bonding motifs in packed bilayers with $-C_8C_4$ tails. Specifically, there is a clear correlation between DG stability and substantial inter-layer H-bonding between the outer sugar hydroxyl groups, *i.e.*, those connected to the C3′ and C4′ carbons. The four glycolipid anomers (α, β-cellobiosides, β-lactosides, β-maltosides) that stabilize DG phases at longer tail lengths have between 17% and 23% of their total inter-layer H-bonding localized to these two hydroxyl groups; DG is not stabilized for molecules with weaker inter-layer H-bonds between these two hydroxyls (α-maltosides, α-lactosides). These findings underscore that designing glycolipids to destabilize zero-curvature LAM phases in favor of DG or other network phases depends critically on tuning intermolecular interactions and achieving an optimal anisotropic molecular shape. Beyond glycolipids, the fundamental design rules outlined here may also be potentially applicable to broader families of amphiphiles including other small-molecule and even polymeric amphiphiles, facilitating the development of DG-forming materials.

## Author contributions

S. D. performed all experimental investigations, data analysis and wrote the manuscript. C. Z. performed all the simulations, prepared all the simulation-related figures and edited the manuscript. T. M. R. and M. A. C. provided mentorship, research direction, and contributed to the writing and editing of the manuscript. T. P. L. and J. I. S. provided helpful discussion and edited the manuscript. The final version of the manuscript was approved by all authors.

## Conflicts of interest

The authors declare no conflict of interest.

## Data availability

All data is available in the supporting information (SI) and raw data files available upon request. Supplementary information: comprehensive details on general experimental protocols; the preparation and characterization of lactosides and maltosides ($^1$H and $^{13}$C NMR spectra); thermal characterization (DSC); phase behavior characterization (SAXS); and copies of NMR spectra for reference. See DOI: https://doi.org/10.1039/d6sc00024j.

## Acknowledgements

The primary funding for this research was provided by the National Science Foundation through the University of Minnesota MRSEC under Award Number DMR-2011401. The utilization of resources at the Advanced Photon Source, a U.S. Department of Energy (DOE) Office of Science User Facility, was made possible through operation by Argonne National Laboratory under Contract No. DE-AC02-06CH11357. SAXS experiments were conducted at Sector 5 which is associated with the DuPont-Northwestern-Dow Collaborative Access Team (DND-CAT). The DND-CAT was supported by DuPont de Nemours, Inc., the Dow Chemical Company, and Northwestern University. Additional SAXS data were also collected at the University of Minnesota Characterization Facility, partially supported by the same MRSEC program (DMR-2011401). https://BioRender.com was used to prepare some parts of the figures.

## References

1 B. Winter, B. Butz, C. Dieker, G. E. Schröder-Turk, K. Mecke and E. Spiecker, Coexistence of both gyroid chiralities in individual butterfly wing scales of Callophrys rubi, *Proc. Natl. Acad. Sci. U. S. A.*, 2015, **112**(42), 12911–12916.
2 J. W. Galusha, L. R. Richey, J. S. Gardner, J. N. Cha and M. H. Bartl, Discovery of a diamond-based photonic crystal structure in beetle scales, *Phys. Rev. E:Stat. Phys., Plasmas, Fluids, Relat. Interdiscip. Top.*, 2008, **77**(5), 050904.
3 V. Saranathan, C. O. Osuji, S. G. Mochrie, H. Noh, S. Narayanan, A. Sandy, E. R. Dufresne and R. O. Prum, Structure, function, and self-assembly of single network gyroid (I 4132) photonic crystals in butterfly wing scales, *Proc. Natl. Acad. Sci. U. S. A.*, 2010, **107**(26), 11676–11681.
4 P. Vukusic and J. R. Sambles, Photonic structures in biology, *Nature*, 2003, **424**(6950), 852–855.
5 B. S. Lazarus, A. Velasco-Hogan, T. Gómez-del Río, M. A. Meyers and I. Jasiuk, A review of impact resistant biological and bioinspired materials and structures, *J. Mater. Res. Technol.*, 2020, **9**(6), 15705–15738.
6 E. Goi, B. P. Cumming and M. Gu, Gyroid "srs" networks: photonic materials beyond nature, *Adv. Opt. Mater.*, 2018, **6**(18), 1800485.
7 S. Khlebnikov and H. W. Hillhouse, Electronic structure of double-gyroid nanostructured semiconductors: perspectives for carrier multiplication solar cells, *Phys. Rev. B:Condens. Matter Mater. Phys.*, 2009, **80**(11), 115316.
8 L. Li, L. Schulte, L. D. Clausen, K. M. Hansen, G. E. Jonsson and S. Ndoni, Gyroid nanoporous membranes with tunable permeability, *ACS Nano*, 2011, **5**(10), 7754–7766.
9 S. Choudhury, M. Agrawal, P. Formanek, D. Jehnichen, D. Fischer, B. Krause, V. Albrecht, M. Stamm and L. Ionov, Nanoporous cathodes for high-energy Li–S batteries from gyroid block copolymer templates, *ACS Nano*, 2015, **9**(6), 6147–6157.
10 L. Germain, C. A. Fuentes, A. W. van Vuure, A. des Rieux and C. Dupont-Gillain, 3D-printed biodegradable gyroid

scaffolds for tissue engineering applications, *Mater. Des.*, 2018, **151**, 113–122.
11 C. Leal, N. F. Bouxsein, K. K. Ewert and C. R. Safinya, Highly efficient gene silencing activity of siRNA embedded in a nanostructured gyroid cubic lipid matrix, *J. Am. Chem. Soc.*, 2010, **132**(47), 16841–16847.
12 S. S. Oh, A. Demetriadou, S. Wuestner and O. Hess, On the origin of chirality in nanoplasmonic gyroid metamaterials, *Adv. Mater.*, 2013, **25**(4), 612–617.
13 H. Lee, J. Kim and M. J. Park, Exploration of complex nanostructures in block copolymers, *Phys. Rev. Mater.*, 2024, **8**(2), 020302.
14 M. Poppe, C. Chen, F. Liu, S. Poppe and C. Tschierske, Formation of a cubic liquid crystalline nanostructure with π-conjugated fluorinated rods on the gyroid minimal surface, *Chem.–Eur. J.*, 2017, **23**(30), 7196–7200.
15 X. Cai, S. Hauche, S. Poppe, Y. Cao, L. Zhang, C. Huang, C. Tschierske and F. Liu, Network phases with multiple-junction geometries at the gyroid–diamond transition, *J. Am. Chem. Soc.*, 2023, **145**(2), 1000–1010.
16 S. M. Sagnella, C. E. Conn, I. Krodkiewska, M. Moghaddam, J. M. Seddon and C. J. Drummond, Ordered nanostructured amphiphile self-assembly materials from endogenous nonionic unsaturated monoethanolamide lipids in water, *Langmuir*, 2010, **26**(5), 3084–3094.
17 M. A. Alam, J. Motoyanagi, Y. Yamamoto, T. Fukushima, J. Kim, K. Kato, M. Takata, A. Saeki, S. Seki and S. Tagawa, "Bicontinuous cubic" liquid crystalline materials from discotic molecules: a special effect of paraffinic side chains with ionic liquid pendants, *J. Am. Chem. Soc.*, 2009, **131**(49), 17722–17723.
18 F. Liu, M. Prehm, X. Zeng, C. Tschierske and G. Ungar, Skeletal cubic, lamellar, and ribbon phases of bundled thermotropic bolapolyphiles, *J. Am. Chem. Soc.*, 2014, **136**(19), 6846–6849.
19 X. Zeng, M. Prehm, G. Ungar, C. Tschierske and F. Liu, Formation of a Double Diamond Cubic Phase by Thermotropic Liquid Crystalline Self-Assembly of Bundled Bolaamphiphiles, *Angew. Chem., Int. Ed.*, 2016, **128**(29), 8464–8467.
20 R. Hashim, A. Sugimura, H. Minamikawa and T. Heidelberg, Nature-like synthetic alkyl branched-chain glycolipids: a review on chemical structure and self-assembly properties, *Liq. Cryst.*, 2012, **39**(1), 1–17.
21 R. Hashim, N. I. Zahid, N. F. K. Aripin, S. Ogawa and A. Sugimura, Dry thermotropic glycolipid self-assembly: A review, *J. Oleo Sci.*, 2018, **67**(6), 651–668.
22 K. Nickmans and A. P. Schenning, Directed self-assembly of liquid-crystalline molecular building blocks for sub-5 nm nanopatterning, *Adv. Mater.*, 2018, **30**(3), 1703713.
23 J. Jennings, B. Green, T. J. Mann, C. A. Guymon and M. K. Mahanthappa, Nanoporous polymer networks templated by gemini surfactant lyotropic liquid crystals, *Chem. Mater.*, 2018, **30**(1), 185–196.
24 Y. Rokhlenko, K. Kawamoto, J. A. Johnson and C. O. Osuji, Sub-10 nm self-assembly of mesogen-containing grafted macromonomers and their bottlebrush polymers, *Macromolecules*, 2018, **51**(10), 3680–3690.
25 Z. Shen, K. Luo, S. J. Park, D. Li, M. K. Mahanthappa, F. S. Bates, K. D. Dorfman, T. P. Lodge and J. I. Siepmann, Stabilizing a Double Gyroid Network Phase with 2 nm Feature Size by Blending of Lamellar and Cylindrical Forming Block Oligomers, *JACS Au*, 2022, **2**(6), 1405–1416.
26 W. Yang, W. Zhang, L. Luo, X. Lyu, A. Xiao, Z. Shen and X.-H. Fan, Ordered structures and sub-5 nm line patterns from rod–coil hybrids containing oligo (dimethylsiloxane), *Chem. Commun.*, 2020, **56**(71), 10341–10344.
27 X. Yu, K. Yue, I.-F. Hsieh, Y. Li, X.-H. Dong, C. Liu, Y. Xin, H.-F. Wang, A.-C. Shi and G. R. Newkome, Giant surfactants provide a versatile platform for sub-10-nm nanostructure engineering, *Proc. Natl. Acad. Sci. U. S. A.*, 2013, **110**(25), 10078–10083.
28 D. Li, Z. Shen, P. Chen, M. K. Mahanthappa, K. D. Dorfman, T. P. Lodge and J. I. Siepmann, Double-Gyroid Network Morphologies Formed by Asymmetric AB1B2 Triblock Amphiphiles over Wide Volume Fraction Range, *JACS Au*, 2025, **5**(7), 3387–3398.
29 M. De Rosa, A. Gambacorta and A. Gliozzi, Structure, biosynthesis, and physicochemical properties of archaebacterial lipids, *Microbiol. Rev.*, 1986, **50**(1), 70–80.
30 G. D. Sprott, Structures of archaebacterial membrane lipids, *J. Bioenerg. Biomembr.*, 1992, **24**, 555–566.
31 T. H. Epps, E. W. Cochran, T. S. Bailey, R. S. Waletzko, C. M. Hardy and F. S. Bates, Ordered network phases in linear poly (isoprene-*b*-styrene-*b*-ethylene oxide) triblock copolymers, *Macromolecules*, 2004, **37**(22), 8325–8341.
32 H. Hückstädt, T. Goldacker, A. Göpfert and V. Abetz, Core–shell double gyroid morphologies in ABC triblock copolymers with different chain topologies, *Macromolecules*, 2000, **33**(10), 3757–3761.
33 L. Jiang, D. Nykypanchuk, V. J. Pastore and J. Rzayev, Morphological behavior of compositionally gradient polystyrene–polylactide bottlebrush copolymers, *Macromolecules*, 2019, **52**(21), 8217–8226.
34 K. Kawamoto, M. Zhong, K. R. Gadelrab, L.-C. Cheng, C. A. Ross, A. Alexander-Katz and J. A. Johnson, Graft-through synthesis and assembly of janus bottlebrush polymers from A-branch-B diblock macromonomers, *J. Am. Chem. Soc.*, 2016, **138**(36), 11501–11504.
35 S. J. Park, G. K. Cheong, F. S. Bates and K. D. Dorfman, Stability of the double gyroid phase in bottlebrush diblock copolymer melts, *Macromolecules*, 2021, **54**(19), 9063–9070.
36 B. Yu, R. Li and R. A. Segalman, Tuning the double gyroid phase window in block copolymers *via* polymer chain conformation near the interface, *Macromolecules*, 2021, **54**(12), 5388–5396.
37 Q. Xie, Y. Qiang and W. Li, Regulate the stability of gyroids of ABC-type multiblock copolymers by controlling the packing frustration, *ACS Macro Lett.*, 2020, **9**(2), 278–283.
38 C. Chen, R. Kieffer, H. Ebert, M. Prehm, R. b. Zhang, X. Zeng, F. Liu, G. Ungar and C. Tschierske, Chirality Induction through Nano-Phase Separation: Alternating Network Gyroid Phase by Thermotropic Self-Assembly of X-Shaped

Bolapolyphiles, *Angew. Chem., Int. Ed.*, 2020, **59**(7), 2725–2729.

39 A. Lehmann, A. Scholte, M. Prehm, F. Liu, X. Zeng, G. Ungar and C. Tschierske, Soft Rectangular Sub-5 nm Tiling Patterns by Liquid Crystalline Self-Assembly of T-Shaped Bolapolyphiles, *Adv. Funct. Mater.*, 2018, **28**(46), 1804162.

40 M. Alaasar, Y. Cao, Y. Liu, F. Liu and C. Tschierske, Switching Chirophilic Self-assembly: From meso-structures to Conglomerates in Liquid and Liquid Crystalline Network Phases of Achiral Polycatenar Compounds, *Chem.–Eur. J.*, 2022, **28**(67), e202201857.

41 K. Borisch, S. Diele, P. Göring, H. Kresse and C. Tschierske, Tailoring thermotropic cubic mesophases: amphiphilic polyhydroxy derivatives, *J. Mater. Chem.*, 1998, **8**(3), 529–543.

42 W. F. N. W. Iskandar, M. Salim, R. Hashim and N. I. Zahid, Stability of cubic phase and curvature tuning in the lyotropic system of branched chain galactose-based glycolipid by amphiphilic additives, *Colloids Surf., A*, 2021, **623**, 126697.

43 M. Salim, W. F. N. Wan Iskandar, M. Patrick, N. I. Zahid and R. Hashim, Swelling of bicontinuous cubic phases in Guerbet glycolipid: Effects of additives, *Langmuir*, 2016, **32**(22), 5552–5561.

44 N. I. Zahid, M. Salim, C. Y. Liew, B. J. Boyd and R. Hashim, Structural investigation and steric stabilisation of Guerbet glycolipid-based cubosomes and hexosomes using triblock polyethylene oxide-polypropylene oxide-polyethylene oxide copolymers, *Colloids Surf., A*, 2022, **648**, 129212.

45 H. Von Minden, K. Brandenburg, U. Seydel, M. Koch, V. Garamus, R. Willumeit and V. Vill, Thermotropic and lyotropic properties of long chain alkyl glycopyranosides. Part II. Disaccharide headgroups, *Chem. Phys. Lipids*, 2000, **106**(2), 157–179.

46 N. N. Saari, A. A. Mislan, R. Hashim and N. I. Zahid, Self-assembly, thermotropic, and lyotropic phase behavior of guerbet branched-chain maltosides, *Langmuir*, 2018, **34**(30), 8962–8974.

47 N. I. Zahid, C. E. Conn, N. J. Brooks, N. Ahmad, J. M. Seddon and R. Hashim, Investigation of the effect of sugar stereochemistry on biologically relevant lyotropic phases from branched-chain synthetic glycolipids by small-angle X-ray scattering, *Langmuir*, 2013, **29**(51), 15794–15804.

48 R. Hashim, S. M. Mirzadeh, T. Heidelberg, H. Minamikawa, T. Yoshiaki and A. Sugimura, A reevaluation of the epimeric and anomeric relationship of glucosides and galactosides in thermotropic liquid crystal self-assemblies, *Carbohydr. Res.*, 2011, **346**(18), 2948–2956.

49 P. Sakya and J. Seddon, Thermotropic and lyotropic phase behaviour of monoalkyl glycosides, *Liq. Cryst.*, 1997, **23**(3), 409–424.

50 K. A. Ishak, N. I. Zahid, T. S. Velayutham, M. S. M. Annuar and R. Hashim, Effects of lipid packing and intermolecular hydrogen bond on thermotropic phase transition of stearyl glucoside, *J. Mol. Liq.*, 2019, **281**, 20–28.

51 D. A. Mannock, M. D. Collins, M. Kreichbaum, P. E. Harper, S. M. Gruner and R. N. McElhaney, The thermotropic phase behaviour and phase structure of a homologous series of racemic β-d-galactosyl dialkylglycerols studied by differential scanning calorimetry and X-ray diffraction, *Chem. Phys. Lipids*, 2007, **148**(1), 26–50.

52 V. Manickam Achari, H. S. Nguan, T. Heidelberg, R. A. Bryce and R. Hashim, Molecular dynamics study of anhydrous lamellar structures of synthetic glycolipids: Effects of chain branching and disaccharide headgroup, *J. Phys. Chem. B*, 2012, **116**(38), 11626–11634.

53 R. Hashim, H. H. A. Hashim, N. Z. M. Rodzi, R. S. D. Hussen and T. Heidelberg, Branched chain glycosides: Enhanced diversity for phase behavior of easily accessible synthetic glycolipids, *Thin Solid Films*, 2006, **509**(1–2), 27–35.

54 S. Das, C. Zheng, T. P. Lodge, J. I. Siepmann, M. K. Mahanthappa, M. A. Calabrese and T. M. Reineke, Self-Assembly of Unusually Stable Thermotropic Network Phases by Cellobiose-Based Guerbet Glycolipids, *Biomacromolecules*, 2024, **25**(2), 1291–1302.

55 P. I. Kuzmin, J. Zimmerberg, Y. A. Chizmadzhev and F. S. Cohen, A quantitative model for membrane fusion based on low-energy intermediates, *Proc. Natl. Acad. Sci. U. S. A.*, 2001, **98**(13), 7235–7240.

56 X. Wang and M. Deserno, Determining the lipid tilt modulus by simulating membrane buckles, *J. Phys. Chem. B*, 2016, **120**(26), 6061–6073.

57 G. Illya, R. Lipowsky and J. Shillcock, Two-component membrane material properties and domain formation from dissipative particle dynamics, *J. Chem. Phys.*, 2006, **125**(11), 114710.

58 S. J. Marrink, A. H. De Vries and D. P. Tieleman, Lipids on the move: simulations of membrane pores, domains, stalks and curves, *Biochim. Biophys. Acta, Biomembr.*, 2009, **1788**(1), 149–168.

59 I. Pascher, Molecular arrangements in sphingolipids Conformation and hydrogen bonding of ceramide and their implication on membrane stability and permeability, *Biochim. Biophys. Acta, Biomembr.*, 1976, **455**(2), 433–451.

60 S. J. Slater, C. Ho, F. J. Taddeo, M. B. Kelly and C. D. Stubbs, Contribution of hydrogen bonding to lipid-lipid interactions in membranes and the role of lipid order: effects of cholesterol, increased phospholipid unsaturation, and ethanol, *Biochemistry*, 1993, **32**(14), 3714–3721.

61 Z. Yu, T. Calvert and D. Leckband, Molecular forces between membranes displaying neutral glycosphingolipids: evidence for carbohydrate attraction, *Biochemistry*, 1998, **37**(6), 1540–1550.

62 C. V. Kulkarni, T.-Y. Tang, A. M. Seddon, J. M. Seddon, O. Ces and R. H. Templer, Engineering bicontinuous cubic structures at the nanoscale—the role of chain splay, *Soft Matter*, 2010, **6**(14), 3191–3194.

63 T. Róg, I. Vattulainen, A. Bunker and M. Karttunen, Glycolipid membranes through atomistic simulations: effect of glucose and galactose head groups on lipid bilayer properties, *J. Phys. Chem. B*, 2007, **111**(34), 10146–10154.

64 X.-M. Li, M. M. Momsen, H. L. Brockman and R. E. Brown, Lactosylceramide: effect of acyl chain structure on phase behavior and molecular packing, *Biophys. J.*, 2002, **83**(3), 1535–1546.

65 P. Pinillos, A. Camiruaga, F. Torres-Hernández, F. J. Basterrechea, I. Usabiaga and J. A. Fernández, Exploring the interaction sites in glucose and galactose using phenol as a probe, *Phys. Chem. Chem. Phys.*, 2023, **25**(10), 7205–7212.

66 Y. Kozlovsky, A. Efrat, D. A. Siegel and M. M. Kozlov, Stalk phase formation: effects of dehydration and saddle splay modulus, *Biophys. J.*, 2004, **87**(4), 2508–2521.

67 V. Kocherbitov and O. Söderman, Glassy crystalline state and water sorption of alkyl maltosides, *Langmuir*, 2004, **20**(8), 3056–3061.

68 T.-Y. D. Tang, N. J. Brooks, O. Ces, J. M. Seddon and R. H. Templer, Structural studies of the lamellar to bicontinuous gyroid cubic (Q GII) phase transitions under limited hydration conditions, *Soft Matter*, 2015, **11**(10), 1991–1997.

69 C. E. Conn, O. Ces, X. Mulet, S. Finet, R. Winter, J. M. Seddon and R. H. Templer, Dynamics of Structural Transformations between Lamellar<? format?> and Inverse Bicontinuous Cubic Lyotropic Phases, *Phys. Rev. Lett.*, 2006, **96**(10), 108102.